ACS APPLIED MATERIALS & INTERFACES

Research Article

www.acsami.org

Lead Sulfide Nanocrystal Quantum Dot Solar Cells with Trenched ZnO Fabricated via Nanoimprinting

Sarah Kim,[†,∥] Jun Kwan Kim,[†,∥] Jianbo Gao,[⊥] Jung Hoon Song,[†,‡] Hey Jin An,[†,#] Tae-Soo You,[#] Tae-Soo Lee,[§] Jong-Ryul Jeong,[§] Eung-Sug Lee,[†] Jun-Ho Jeong,[†] Matthew C. Beard,[⊥] and Sohee Jeong*[,†]

[†]Nanomechanical Systems Research Division, Korea Institute of Machinery and Materials, Yuseong-gu, Daejeon, 305-343, Korea

[⊥]National Renewable Energy Laboratory, Colorado 80401, United States

[§]Department of Materials Science and Engineering, Graduate School of Green Energy Technology, Chungnam National University, Daejeon 305-764 Korea

[‡]Graduate School of Nanoscience and Technology (WCU), KAIST, Daejeon 305-701, Korea

[#]Department of Chemistry, Chungbuk National University, Chungbuk, 361-763, Korea

ABSTRACT: The improvement of power conversion efficiency, especially current density (J_{sc}), for nanocrystal quantum dot based heterojunction solar cells was realized by employing a trenched ZnO film fabricated using nanoimprint techniques. For an optimization of ZnO patterns, various patterned ZnO films were investigated using electrical and optical analysis methods by varying the line width, interpattern distance, pattern height, and residual layer. Analyzing the features of patterned ZnO films allowed us to simultaneously optimize both the pronounced electrical effects as well as optical properties. Consequently, we achieved an enhancement in J_{sc} from 7.82 to 12.5 mA cm^{-2} by adopting the patterned ZnO with optimized trenched shape.

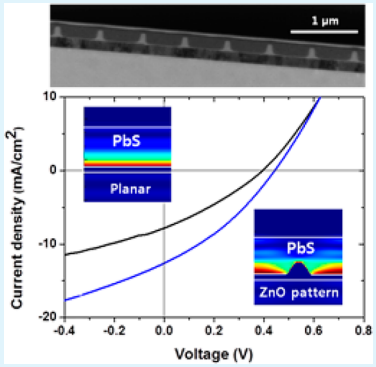

KEYWORDS: *quantum dot solar cells, lead sulfide quantum dots, nanoimprinting, patterned ZnO, depleted heterojunction, nanostructured interface*

INTRODUCTION

Nanocrystal quantum dot (NQD)-based photovoltaics (PVs) are of great interest due to low-cost solution processability and quantum size-effect-originated tunability that allows matching absorption with the solar spectrum in third generation PV devices.[1,2] To date, progress in NQD based PV device performance has been achieved through the innovations of PV device architecture and ligand-passivation stratagem. Indeed, lead sulfide (PbS) NQD-based solar cells fabricated using assembled NQD arrays have rapidly advanced in recent years, from the first report of PbS Schottky-junction devices to recent reports of 5.1% power conversion efficiency (PCE) for an atomic passivated NQD-based solar cell with a depleted heterojunction (DH) architecture.[3,4] Meanwhile, further improvement of PCE of 7% using organic−inorganic hybrid passivated NQDs as a light-absorbing layer in DH solar cell was reported by Ip et al.[5] Although assembled NQD based PV reached above 7% PCE with the advent of the DH architecture and a proper ligand passivation, the engineering of device architecture in order to maximize the absorption of incident photons is still a challenging issue that should lead to further enhancements in PCE. In practice, enhancing photon absorption from a given amount of colloidal NQD solid offers significant benefits for increasing the available photocurrent.[6] Nanostructured interfaces between *n*- and *p*-type semiconductor materials leads to the improvement of electron extraction by allowing a greater amount of light absorption. Recent reports have demonstrated that an actual short-circuit current density (J_{sc}) enhancement approaching 30% relative to a planar device could be obtained using a device with the nanostructured TiO_2 that enhances absorption without compromising carrier extraction.[7] Moreover, a much higher open-circuit voltage (V_{oc}) could also be achieved by employing the TiO_2 nanopillars in comparison with the planar device.[8] Consequently, an employment of nanostructured electrodes such as TiO_2 and ZnO which are generally used as *n*-type semiconducting materials in PbS NQD-based heterojunction device is an appropriate stratagem toward enhancing PCE of the PV device.[9,10] It is noteworthy that it would be desirable to construct a nanostructured electrode in which the NQD film remains still fully depleted in order to maximize the efficiency of incident photon absorption and extraction in an NQD-based PV device.[7]

Received: February 3, 2013
Accepted: April 12, 2013
Published: April 12, 2013

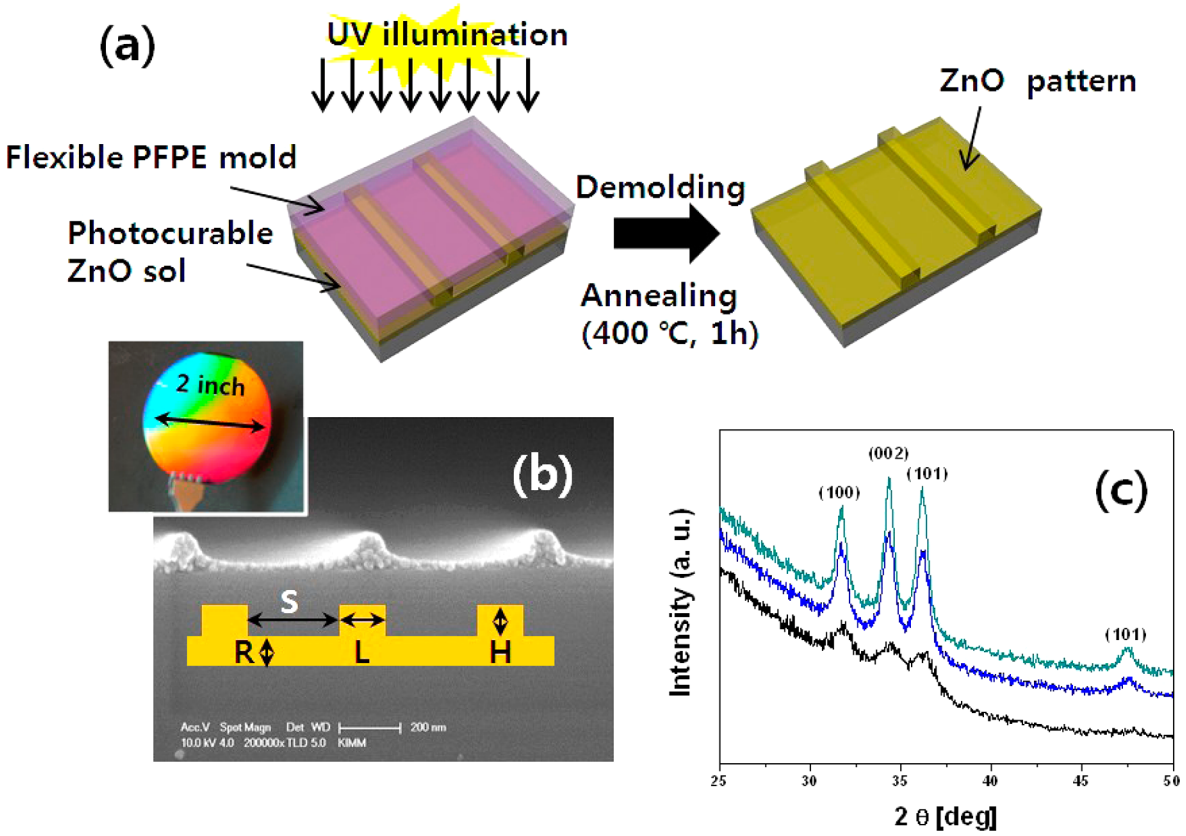

Figure 1. (a) Scheme for the ZnO pattern prepared single step UV imprinting. A photosensitive precursor solution was spin coated on the substrate followed by direct nanoimprinting with a PFPE flexible mold whose pattern period was within 400−1000 nm. After demolding and annealing, the ZnO line pattern was formed on the substrate. (b) Cross-sectional SEM image of ZnO line pattern and depicted structure. This process is patternable for a large area above 2 in. (c) ZnO XRD data with respect to postannealing temperature (black 300 °C, blue 400 °C, green 500 °C for 1 h, respectively).

Previously, TiO_2 or ZnO nanostructure have been made using a variety of techniques including doctor blade spreading of paste,[11] spray pyrolysis,[12] and nanowire growth[13] in photovoltaic cells. However, these methods have a limit for preparing a regular structure reproducibly. Unlike above-mentioned techniques, direct metal oxide nanoimprint lithography (NIL) using photosensitive sol−gel precursor, which has been recently introduced as a high resolution, high throughput, and low cost patterning tool, open up new routes to fabricate an ordered structured electrode.[14−16] This is highly appropriate to form structured metal oxide layers that should include the residual layer inevitably using the single step process without any etching or deposition step.[17,18]

In this work, we used a direct UV nanoimprint process in order to enable precise, large area, and nanoscale patterning of ZnO for *n*-type layer in PbS NQD-based heterojunction solar cell. For a better understanding of the physical processes in the devices, we studied the optical and electrical effect of the periodic feature of patterned semiconducting structure on the PV performance, and these parameters are investigated theoretically and experimentally in this paper. In our PbS NQD-based solar cell with nanopatterned ZnO structure, we find that, while the optical enhancement is minimal, the electrical effect is pronounced, resulting in the enhancement of J_{sc} over 50% in comparison with planar structures.

EXPERIMENTAL METHODS

Synthesis Procedure of Photosensitive Sol and Fabrication of ZnO Line Pattern. The photocurable ZnO sol in the present study were synthesized by zinc acetate, 2-methoxyethanol, and ethanolamine was used as a solvent and stabilizer. Also, photosensitive 2-nitrobenzaldehyde was added into the solution precursors and contributed to form a cross-linked network structure via photochemical reaction. UV curable inorganic precursor including zinc acetate was used as material for fabricating patterned *n*-type layer in the QD solar cell process. First, the photosensitive precursor film was spin-coated on the ITO substrate at 3000−5000 rpm. Film thickness was controlled by modulating the concentration of sol and spin coating speed. Flexible PFPE mold duplicated from an Si master which has a line shape with various periods was then pressed against the ZnO precursor film at a pressure of 3 bar for 5 min using a homemade UV nanoimprintor. After demolding, an additional 10 min of UV light (52 mW cm^{-2} with a major wavelength peak of 365 nm) illuminated the ZnO pattern. Finally, the ZnO trench pattern was annealed at 400 °C for 1 h in order to remove residual organic compounds. With UV irradiation and annealing, the thickness of the ZnO films was reduced by elimination of trapped organic molecules inside the film which originated from the decomposition of precursors during the photochemical reaction. Upon annealing, the height of the ZnO line pattern decreased from 350 to 100 nm in the crystalline phase. Despite this significant shrinkage, macroscopically uniform and crack-free patterned structure was obtained and an isotropic volume loss was observed.

Device Fabrication. In order to assemble PbS NQD solids, a layer-by-layer dip-coating method was employed. The substrate was first dipped into PbS NQDs dispersed in hexane followed by a subsequent ligand-exchange using 1, 2-ethanedithiol (EDT) to reduce

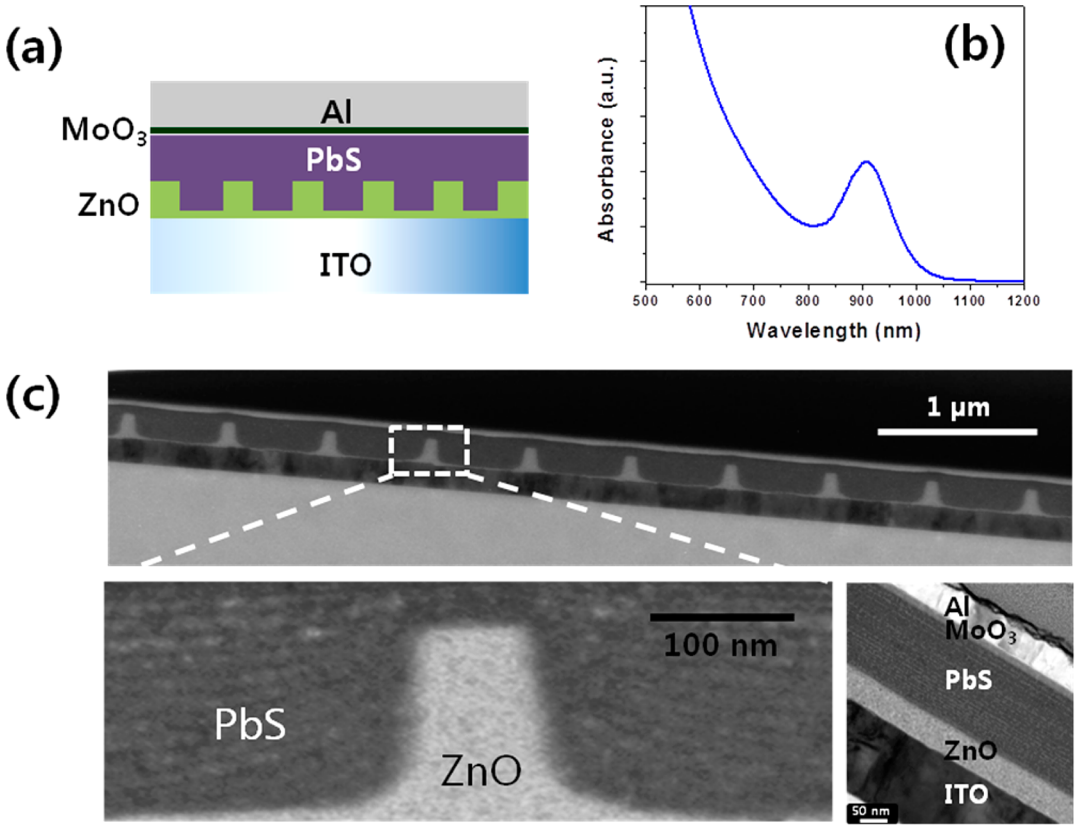

Figure 2. (a) Illustrated QD solar cell structure with ZnO line-pattern. (b) Absorbance of PbS QD with first excitonic transition peak at 910 nm. (C) High-resolution cross-sectional TEM images of fully fabricated device with patterned (left) and planar ZnO films (bottom-right corner). NQD layers formed on the ZnO/ITO substrate without any void or defects followed by MoO_3 and Al deposition.

inter-NQDs distance. These steps were repeated to obtain the desirable film-thickness. Finally, heterojunction solar cells were completed by employing 180 nm-Al and 10 nm-MoO_3 thin layers on the top of PbS NQDs solids as a top electrode using thermal evaporation technique.

RESULTS AND DISCUSSION

Figure 1 schematically describes the procedure for ZnO patterning as the efficient electron collecting layer in the DH NQD solar cell. ZnO line-pattern with various periods were duplicated from predesigned Si master by the following process. First, a ZnO precursor solution including a photosensitive nitrobenzaldehyde was spin-coated onto substrate in order to assist cross-linking by UV. Then, UV direct nanoimprinting employing a soft PFPE (bifunctional urethane methacrylate perfluoropolyether) mold with a low surface energy formed the ZnO line pattern with periods of 400−1000 nm by a single step method as shown in Figure 1.

The inset of Figure 1b shows reflected color by large-area ZnO pattern successfully created onto the 2 in. Si wafer. Subsequently thermal annealing at 400 °C for 1 h improved the crystallinity of the ZnO film. Additionally, this step removed any byproducts after cross-linking and densified the remaining imprinted ZnO patterns. We depict this design (L line width, S interpattern distance, H pattern height, R residual layer) in its realized SEM image of Figure 1b. Also, for optimization of ZnO crystallinity, we analyzed X-ray diffraction (XRD) for the ZnO films annealed at various annealing temperatures. As annealing temperature increased from 300 to 500 °C, ZnO crystallinity is enhanced, as indicated by the intensity of (002) peak relative is to the intensity of the other peaks i.e., (100) and (101). We carried out the annealing process at the annealing temperature of 400 °C because the sheet resistance of ITO films increased significantly when it annealed over 400 °C leading to the increase of series resistance in the PV device.

Figure 2a shows the schematic structure of the PbS NQD-based heterojunction device. As shown in Figure 2a, the heterojunction PV device is fabricated with Al/MoO_3/PbS/ZnO/ITO structure. To help achieve efficient exciton dissociation and electron transport, we used ZnO line patterns.[19−21] Minimum-residual layer of 30 nm was required to prevent shunting between the PbS film and ITO as well as effective carrier separation at the interface.[24]

PbS NQDs were synthesized and purified as previously reported.[22] Figure 2b shows the absorption spectrum of as-synthesized PbS NQDs dispersed in tetrachloroethylene (TCE). First excitonic transition occurred at 910 nm corresponding to the optical band gap of 1.4 eV. The PbS NQD film was deposited onto the ZnO film via a dip-coating method using PbS NQDs in hexane (concentration 10 mg mL^{-1}) and the subsequent ligand-exchange process was performed using ethanedithiol (EDT) in acetonitrile to further enhance the electronic coupling among NQDs by creating closed-packed NQD assemblies.[23] These layer-by-layer (LBL) coating procedures were repeated until the desirable thickness. For a fully depleted structure, ∼200 nm of PbS NQD films were fabricated.[9,24] Finally, the PbS NQD-based heterojunction solar cell was completed by depositing 180 nm-Al and 10 nm-MoO_3 films on top of the PbS NQD film using a thermal evaporator system. The transition metal oxide layer can be used as an electron blocking layer (EBL) in the heterojunction

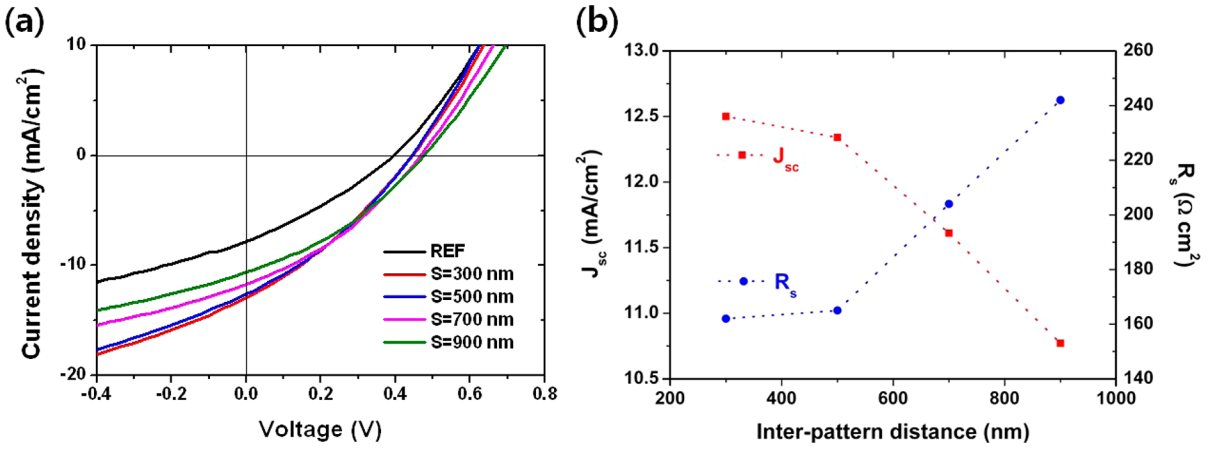

Figure 3. (a) *J*–*V* characteristics of PbS NQDs-based heterojunction solar cells fabricated on the patterned ZnO films with different interpattern distances. (b) Dependence of the interpattern distance on short-circuit current density (J_{sc}, red) and series resistance (R_s, blue).

Table 1. Photovoltaic Parameters of Planar and Devices with ZnO Line Patterns[a]

	line (L, nm)	space (S, nm)	height (H, nm)	residual layer (R, nm)	V_{oc} (mV)	J_{sc} (mA/cm^2)	FF (%)	PCE (%)
device 1	100	300	100	35	448.6	12.5	31.25	1.78
device 2	100	500	100	43	448.5	12.34	33.65	1.90
device 3	100	700	100	47.5	461.4	11.61	33.27	1.81
device 4	100	900	100	50	476.6	10.77	33.8	1.76
device 5	100	300	50	47.5	445.3	10.76	29.5	1.43
planar				60	394.3	7.82	29.9	0.92

[a]The data were obtained by averaging 3–6 measurements.

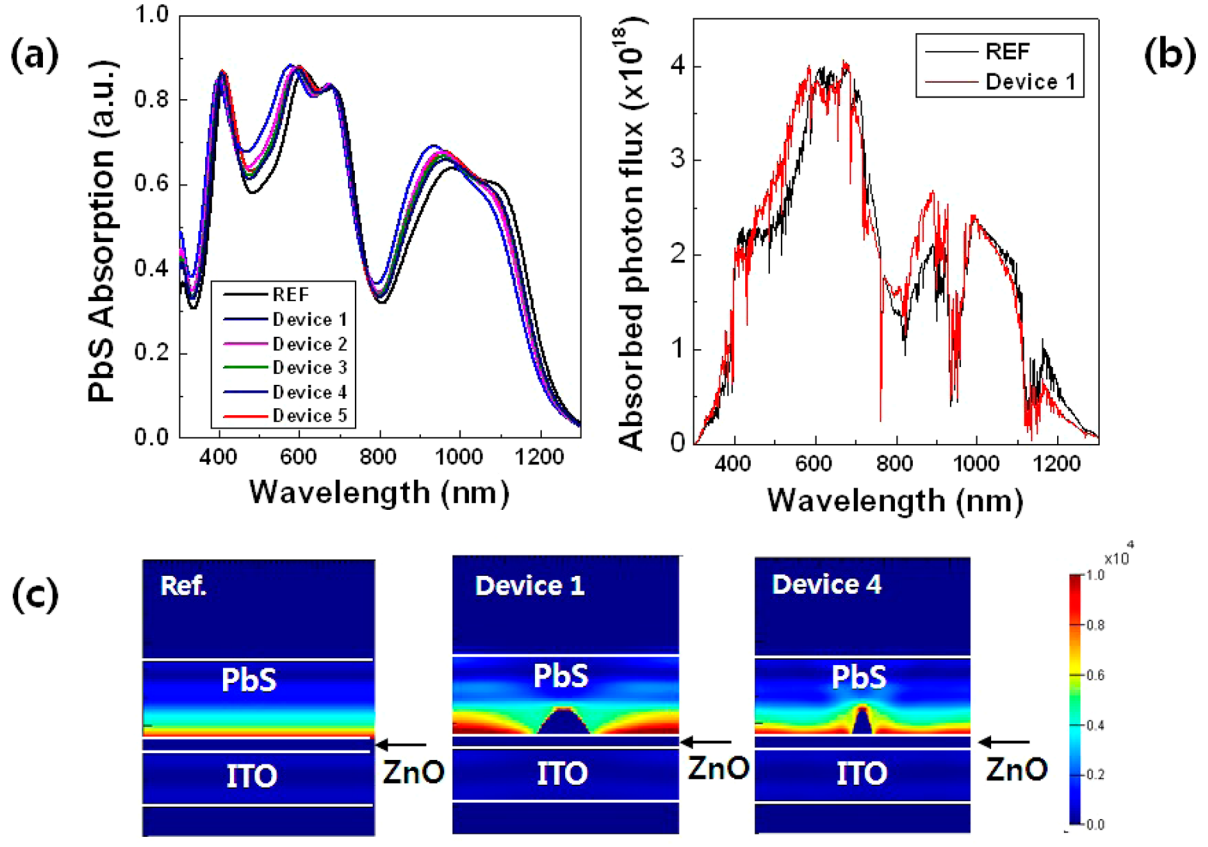

Figure 4. (a) Absorption spectra in PbS layer for reference and device 1–5. (b) Absorbed photon flux in PbS layer for reference and device 1. (c) Electric field intensity distribution |*E*| of QD solar cell for illumination at λ = 500 nm for reference, device 1, and device 4.

device, resulting in the effective blocking of the back transferred electrons from the junction area as recently proposed by Gao et al.[24]

Figure 2c shows high-resolution cross-sectional transmission electron microscopy (HR-TEM) images of a fully fabricated device with nanopatterned and planar ZnO films, respectively. It can be clearly observed that the trench-shaped ZnO film formed by the nanoimprinting method is periodically ordered on the ITO substrate. The ZnO line pattern was replicated by the direct UV nanoimprinting using the PFPE mold. Parallel lines with 100 nm in height, 100 nm in width, and 500 nm in space were achieved after annealing at 400 °C for 1 h. Moreover, a smooth interface without any voids and/or dislocations was formed between PbS film and ZnO film as well as the top electrode/PbS interface as shown in Figure 2c. It is also observed that close-packed PbS NQD film is deposited in this work. The measured current density−voltage (J−V) characteristics of representative devices under 100 mW/cm^2 AM 1.5 G solar illumination are shown in Figure 3a. The overall effect of the interpattern distance of ZnO films on the device performance originates from the variation of the short-circuit current density (J_{sc}) and the series resistance (R_s) as shown in Figure 3b. Here, we examined six devices per fixed interpattern distance, and then the calculated average parameters including J_{sc} and R_s were plotted in Figure 3b. While the V_{oc} slightly increases, the J_{sc} decreases with increasing interpattern distance. We note that the thickness of residual ZnO layer increases from 35 to 50 nm as the interpattern distance increases ranging from 300 to 900 nm, resulting in the increase of series resistance and the reduction of photo-generated carrier density. From these results, we can deduce that the decrease of J_{sc} is not only attributed to the decrease of the junction area but also the increase of residual ZnO layer thickness. The effects of the pattern feature size on the photovoltaic performance are shown in Table 1. Table 1 lists the photovoltaic parameters including J_{sc}, V_{oc}, the fill factor (FF), and the overall PCE according to pattern feature size. Fill factors are influenced by series resistance as well as the diode ideality factor.[25,26] Since a decrease in the ZnO period results in a proportional increase in the junction area between PbS NQDs and ZnO, we can expect that charge collection increase against capture of photogenerated carriers in the quantum dot film result in increased J_{sc}. Here, a slight increase of V_{oc} should be concerned with the reduction of reverse saturation current in the device.

In order to elucidate the effect of optical absorption on the enhanced PCE shown in Table 1, a three-dimensional finite-difference time-domain (FDTD) method was used to theoretically calculate the optical absorption in the PbS layer. The device architecture shown in Figure 2a was used and the device is illuminated with a linearly polarized plane wave, which propagates from the ITO to Al layer. A grid size of 0.1 nm was used in this simulation. Figure 4 shows simulated absorption spectra as well as absorbed photon flux in PbS layer for the reference (planar) and device 1−5. The absorbed photon flux was calculated by multiplying the absorption in PbS layer (Figure 4a) with the AM1.5 solar spectral irradiance. Figure 4b clearly shows that the number of the absorbed photon in the PbS layer is increased especially in the ranges 400−600 and 800−900 nm. Even though we cannot calculate an exact number of generated carriers by increased photon absorption due to a nonconstant multiplication yield, the improved light absorption partially attributed to the enhanced efficiency in the nanostructured QD solar cells. Figure 4c shows electromagnetic field intensity distribution in the solar cell device at 500 nm which reveals the electromagnetic field enhancement in the PbS layer.

However, following the argument above, the increased absorption over the planar structure is not enough to explain the observed increase in current density. This may imply that optical properties have a minor effect for the change of J_{sc} or that such effects are overwhelmed by electrical properties according to ZnO specific area. To obtain additional insight into the device performance, we plot the correlation between normalized ZnO surface area and measured J_{sc} in Figure 5. The

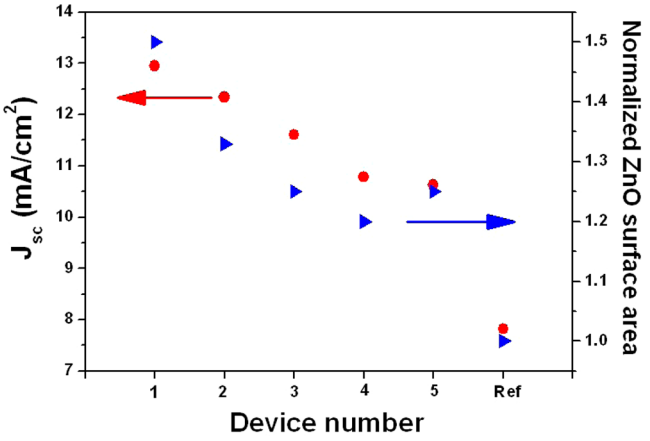

Figure 5. Dependence of the interpattern distance on short-circuit current density (J_{sc}) and ZnO surface area.

good correlation indicates that the higher surface area contributes to the higher J_{sc}. The ratio of the J_{sc} value for the 400 nm and 1 μm period electrodes (1.16) was smaller than the ratio of the specific area of the electrodes (1.25), which is likely due to an increased rate of recombination or increase of series resistance by increased residual layer.

CONCLUSIONS

In conclusions, the effects of nanoimprinted ZnO films with various configurations on the performance of NQD-based solar cells were investigated using electrical and optical analysis methods. A decrease in the interpattern distance of ZnO results in a proportional increase in the junction area between PbS NQDs and ZnO allowing an increase in the charge collection against the capture of photogenerated carriers in the quantum dot film results in increased J_{sc}. Moreover, we can deduce that the slight increase of optical absorption in the visible (400−600 nm) and near-infrared regions (800−900 nm) should affect the enhancement of solar cell performance from FDTD data. Indeed, over 1.5 times higher J_{sc} of 12.5 mA cm^2 was obtained for patterned ZnO fabricated with optimized features compared to those fabricated with a planar surface. Therefore, an improvement of solar cell performance could be realized by employing the patterned ZnO films fabricated using the single-step nanoimprinting method.

AUTHOR INFORMATION

Corresponding Author

*E-mail: sjeong@kimm.re.kr.

Author Contributions

‖S.K. and J.K.K.: These authors contributed equally.

Notes

The authors declare no competing financial interest.

■ ACKNOWLEDGMENTS

This work was supported by the Global Frontier R&D Program by the Center for Multiscale Energy Systems funded by the National Research Foundation (NRF) under the Ministry of Education, Science, and Technology (2011-0031566) and the basic research fund from KIMM. T.-S.L. and J.-R.J. were supported by the NRF (No. 2012-043865). J.G. and M.C.B. were supported by the Center for Advanced Solar Photophysics, an Energy Frontier Research Center funded by the US Department of Energy (DOE), Office of Science, Office of Basic Energy Sciences. DOE funding was provided to the NREL through Contract No. DE-AC36-08G028308.

■ REFERENCES

(1) Sargent, E. H. *Nat. Photonics* **2009**, *3*, 325−331.
(2) Kramer, I. J.; Sargent, E. H. *ACS Nano* **2011**, *5*, 8506−8514.
(3) Mcdonald, S. A.; Konstantatos, G.; Zhang, S.; Cyr, P. W.; Klem, E. J. D.; Levina, L.; Sargent, E. H. *Nat. Mater.* **2005**, *4*, 138−142.
(4) Pattantyus-Abraham, A. G.; Kramer, I. J.; Barkhouse, A. R.; Wang, X.; Konstantatos, G.; Debnath, R.; Levina, L.; Raabe, I.; Nazeeruddin, M. K.; Gratzel, M.; Sargent, E. H. *ACS Nano* **2010**, *6*, 3374−3380.
(5) Ip, A. H.; Thon, S. M.; Hoogland, S.; Voznyy, O.; Zhitomirsky, D.; Debnath, R.; Levina, L.; Rollny, L. R.; Carey, G. H.; Fischer, A.; Kemp, K. W.; Kramer, I. J.; Ning, Z.; Labelle, A. J.; Chou, K. W.; Amassian, A.; Sargent, E. H. *Nat. Nanotechnol.* **2012**, *7*, 577−582.
(6) Sargent, E. H. *Nat. Photonics* **2012**, *6*, 133−135.
(7) Barkhouse, D. A. R.; Debnath, R.; Kramer, I. J.; Zhitomirsky, D.; Pattantyus-Abraham, A. G.; Levina, L.; Etgar, L.; Gratzel, M.; Sargent, E. H. *Adv. Mater.* **2011**, *23*, 3134−3138.
(8) Kramer, I. J.; Zhitomirsky, D.; Bass, J. D.; Rice, P. M.; Topuria, T.; Krupp, L.; Thon, S. M.; Ip, A. H.; Debnath, R.; Kim, H. C.; Sargent, E. H. *Adv. Mater.* **2012**, *24*, 2315−2319.
(9) Brown, P. R.; Lunt, R. R.; Zhao, N.; Osedach, T. P.; Wanger, D. D.; Chang, L. Y.; Bawendi, M. G.; Bulovic, V. *Nano Lett.* **2011**, *11*, 2955−2961.
(10) Lee, J. M.; Park, J. S.; Lee, S. H.; Kim, H.; Yoo, S.; Kim, S. O. *Adv. Mater.* **2011**, *23*, 629−633.
(11) Arango, A. C.; Carter, S. A.; Brock, P. J. *Appl. Phys. Lett.* **1999**, *74*, 1698−1700.
(12) Huisman, C. L.; Schoonman, A. G. J. *Chem. Mater.* **2003**, *15*, 4617−4624.
(13) Leschkies, K. S.; Jacobs, A. G.; Norris, D. J.; Aydil, E. S. *Appl. Phys. Lett.* **2009**, *95*, 1931031−1931033.
(14) Park, H. H.; Choi, D. G.; Zhang, X.; Jeon, S.; Park, S. J.; Lee, S. W.; Kim, S.; Kim, K. D.; Choi, J. H.; Lee, J.; Yun, D. K.; Lee, K. J.; Park, H. H.; Hill, R. H.; Jeong, J. H. *J. Mater. Chem.* **2010**, *20*, 1921−1926.
(15) Park, H.-H.; Zhang, X.; Lee, S. W.; Kim, K. D.; Choi, D. G.; Choi, J. H.; Lee, J.; Lee, E. S.; Park, H. H.; Hill, R. H.; Jeong, J. H. *J. Mater. Chem.* **2011**, *21*, 657−662.
(16) Hampton, M. J.; S. S. Zhou, W.; Nunes, Z. J.; Ko, D. H.; Templeton, J. L.; Samulski, E. T.; DeSimone, J. M. *Adv. Mater.* **2008**, *20*, 2667−2673.
(17) Kim, S.; Kim, S. M.; Park, H. H.; Jung, J. W.; Jeong, J. H.; Jeong, J. R. *Opt. Express* **2012**, *20*, A713−A721.
(18) Kim, S.; Shin, D. O.; Choi, D. G.; Jeong, J. R.; Mun, J. H.; Yang, Y. B.; Kim, J. U.; Kim, S. O.; Jeong, J. H. *Small* **2012**, *8*, 1563−1569.
(19) Choi, J.; Terazima, M. *J. Phys. Chem. B* **2003**, *107*, 9552−9557.
(20) Diaspro, A.; Federici, F.; Viappiani, C.; Krol, S.; Pisciotta, M.; Chirico, G.; Cannone, F.; Gliozzi, A. *J. Phys. Chem. B* **2003**, *107*, 11008−11012.
(21) Seo, H. O.; Park, S. Y.; Shim, W. H.; Kim, K. D.; Lee, K. H.; Jo, M. Y.; Kim, J. H.; Lee, E.; Kim, D. W.; Kim, Y. D.; Lim, D. C. *J. Phys. Chem. C.* **2011**, *115*, 21517−21520.
(22) Baik, S. J.; Kim, K.; Lim, K. S.; Jung, S. M.; Park, Y. C.; Han, D. G.; Lim, S.; Yoo, S.; Jeong, S. *J. Phys. Chem. C* **2011**, *115*, 607−612.
(23) Jeong, K. S.; Tang, J.; Liu, H.; Kim, J.; Schaefer, A. W.; Kemp, K.; Levina, L.; Wang, X.; Hoogland, S.; Debnath, R.; Brzozewski, L.; Sargent, E. H.; Asbury, J. B. *ACS Nano* **2012**, *1*, 89−99.
(24) Gao, J.; Perkins, C. L.; Luther, J. M.; Hanna, M. C.; Chen, H. Y.; Semonin, O. E.; Nozik, A. J.; Ellingson, R. J.; Beard, M. C. *Nano Lett.* **2011**, *11*, 3263−3266.
(25) Kippelen, B.; Bredas, J. L. *Energy Environ. Sci.* **2009**, *2*, 251−261.
(26) Stevens, D. M.; Speros, J. C.; Hillmyer, M. A.; Frisbie, D. F *J. Phys. Chem. C* **2011**, *115*, 20806−20816.